

Influence of concurrent horizontal and vertical ground excitations on the collapse margins of non-ductile RC frame buildings

E. Noroozinejad Farsangi^{1a}, T.Y. Yang^{*2,3} and A.A. Tasnimi^{4b}

¹SERC, International Institute of Earthquake Engineering and Seismology, Tehran, Iran

²International Joint Research Laboratory of Earthquake Engineering, Shanghai, China

³Department of Civil Engineering, University of British Columbia, Vancouver, Canada

⁴Department of Civil and Environmental Engineering, Tarbiat Modares University, Tehran, Iran

(Received January 13, 2016, Revised May 20, 2016, Accepted June 10, 2016)

Abstract. Recent earthquakes worldwide show that a significant portion of the earthquake shaking happens in the vertical direction. This phenomenon has raised significant interests to consider the vertical ground motion during the seismic design and assessment of the structures. Strong vertical ground motions can alter the axial forces in the columns, which might affect the shear capacity of reinforced concrete (RC) members. This is particularly important for non-ductile RC frames, which are very vulnerable to earthquake-induced collapse. This paper presents the detailed nonlinear dynamic analysis to quantify the collapse risk of non-ductile RC frame structures with varying heights. An array of non-ductile RC frame archetype buildings located in Los Angeles, California were designed according to the 1967 uniform building code. The seismic responses of the archetype buildings subjected to concurrent horizontal and vertical ground motions were analyzed. A comprehensive array of ground motions was selected from the PEER NGA-WEST2 and Iran Strong Motions Network database. Detailed nonlinear dynamic analyses were performed to quantify the collapse fragility curves and collapse margin ratios (CMRs) of the archetype buildings. The results show that the vertical ground motions have significant impact on both the local and global responses of non-ductile RC moment frames. Hence, it is crucial to include the combined vertical and horizontal shaking during the seismic design and assessment of non-ductile RC moment frames.

Keywords: non-ductile RC frame; collapse margin; fragility curves; vertical excitation; OpenSees

1. Introduction

With increasing population and infrastructure in earthquake prone areas worldwide, many urban cities are facing an increasing seismic risk (Eskandari *et al.* 2015, Zhang *et al.* 2015). Non-ductile concrete frames designed and constructed prior to the introduction of modern seismic design provisions are especially vulnerable to earthquake shaking (Galal 2007). These type of

*Corresponding author, Professor, E-mail: yang@ilee-tj.com, yang@civil.ubc.ca

^aPh.D. Researcher, E-mail: e.noroozinejad@iiees.ac.ir

^bProfessor, E-mail: tasnimi@modares.ac.ir

structural systems have experienced significant structural and non-structural component damages during the 1971 San Fernando earthquake, 1979 Imperial Valley earthquake, 1987 Whittier Narrows earthquake, and 1994 Northridge earthquake (Papazoglou *et al.* 1996, Wen *et al.* 2004, Bommer *et al.* 2005, Liel *et al.* 2008). To quantify the seismic vulnerability of these non-ductile RC frames, Liel *et al.* (2011), Liel *et al.* (2008) conducted a series of analytical simulation. Their result shows that older concrete buildings are more likely to be damaged in earthquakes, which will incur more repair costs. In addition, older RC frames have 40 times higher annual risk towards collapse compared to modern code-conforming concrete frames. These studies provided valuable insight towards the understanding of the seismic vulnerability of non-ductile RC frames. However, the true seismic vulnerability caused by the vertical ground motion excitation was not considered.

Currently, the vertical component of the earthquake shaking is considered to be only a fraction (typically between 1/2 to 2/3) of the horizontal component shaking. It is usually ignored during the seismic design and assessment of the buildings. However, acceleration records from the 1989 Loma Prieta earthquake, 1994 Northridge earthquake, 1995 Kobe earthquake and 2011 Christchurch earthquake showed that the magnitudes of the vertical component can be as large, or exceed, the horizontal component (Collier *et al.* 2001, Bozorgnia *et al.* 2004). Hence, the assumption to ignore the vertical ground motion during the seismic design and assessment may be incorrect and not conservative.

The objective of this study is to evaluate the seismic vulnerability of older RC frame buildings located in Los Angeles, California when subjected to combined horizontal and vertical excitations. An array of archetype buildings was designed according to the 1967 Uniform Building Code (UBC 1967). The seismic responses of the archetype buildings subjected to concurrent horizontal and vertical ground motions were analyzed. A comprehensive array of ground motions was selected from the PEER NGA-WEST2 database (Ancheta *et al.* 2013), and Iran Strong Motions Network retrieved from (<http://smd.bhrc.ac.ir/Portal/en/Search/Waveforms>). Detailed nonlinear incremental dynamic analysis were performed to quantify the collapse fragility curves and collapse margin ratios (CMRs) of the archetype buildings. The result shows that the peak vertical ground acceleration to peak horizontal ground acceleration ratio decreases as the distance from the Epicenter increases. This is a characteristic of the ground motion, where the P-waves dies down quickly as the wave travel away from the Epi Center. The results of the incremental dynamic analysis show that CMRs are 50% higher when vertical ground motion are not considered. In addition, as the number of story increases, the probability of collapse increases. The probability of collapse is higher when the vertical ground motions are included. Hence it is crucial to include the combined vertical and horizontal excitations when quantify the CMR and probability of collapse for non-ductile RC buildings.

2. Description of the archetype buildings

To analyze the seismic vulnerability of the non-ductile reinforced concrete moment resisting frame (RC-MRFs) building, a set of archetype buildings (as shown in Fig. 1) located in Los Angeles, California was designed according to the 1967 Uniform Building Code (UBC 1967). The prototype building includes two-, five- and nine-story non-ductile RC frame buildings. The reason for choosing this type of construction is because this type of construction is prevalent in California and is highly vulnerable to earthquake shaking (Anagnos *et al.* 2008, Prager *et al.* 2009). Table 1 shows the dimensions and steel reinforcement of the structural columns and beams of the

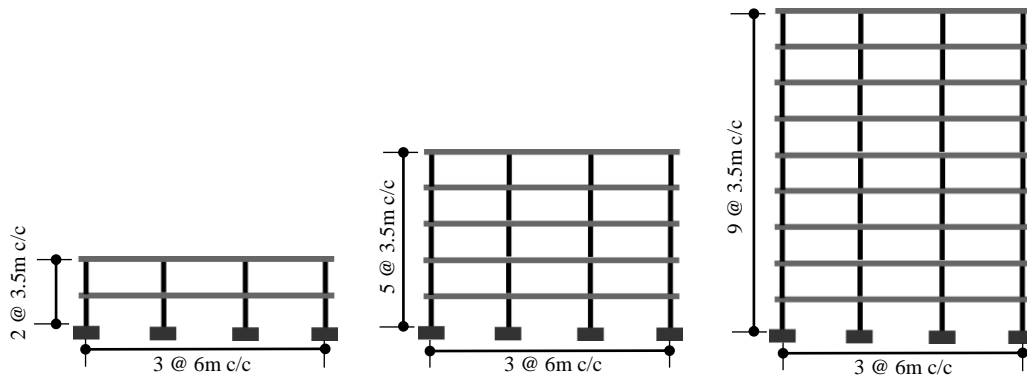


Fig. 1 Schematic representation of the prototype buildings

Table 1 Summary of the structural element sizes and reinforcements details

Model	Storey	Column size ¹ (cm×cm)	Column Reinforcement Ratio, ρ	Column tie Spacing ^{2,3} (cm)	Beam Size ⁴ (m×m)	Beam Reinforcement Ratios ρ (ρ')	Beam Tie Spacing (cm)
2S-MRF	1-2	50×50	0.021	30	50×60	0.008(0.014)	30
5S-MRF	1-3	65×65	0.023	30	50×60	0.007(0.012)	30
	4-5	50×50	0.019	30	50×50	0.008(0.015)	30
9S-MRF	1-4	80×80	0.028	30	60×70	0.006(0.012)	30
	5-7	70×70	0.025	30	60×60	0.007(0.011)	30
	8-9	55×55	0.017	30	50×60	0.006(0.011)	30

Table 2 Modal period of the archetype structures

RC-MRF	$T_1(H)$, (sec.)	$T_2(H)$, (sec.)	$T_3(H)$, (sec.)	$T_1(V)$, (sec.)
2 Storey	0.98	0.46	-	0.12
5 Storey	1.21	0.63	0.21	0.17
9 Storey	1.49	0.68	0.23	0.23

prototype buildings. Masses were calculated and assigned as lump masses at the nodes. Table 2 shows the modal periods of the prototype buildings extracted from eigenvalue analyses. The results show the first translational mode, $T_1(H)$, ranges from 0.98 sec to 1.49 sec. On the other hand, the first vertical vibration model ranges from 0.12 sec to 0.23 sec. This shows the natural vibration period of the structure in the vertical direction, $T_1(V)$, is much shorter than the horizontal direction.

3. Characteristics of the ground motions

The vertical component of the ground motion is associated with the P -waves, while the horizontal components are mainly caused by the S -waves. The wavelength of the P -waves is shorter than that of the S -waves, which means that the former is associated with higher

frequencies. In the near-fault region, ground motion is characterized mainly by source spectra. The *P*-wave spectrum has a higher corner frequency than that of the *S*-wave. *P* and *S* corner frequencies gradually move to lower frequencies as waves propagate away from the source and, as a result, the vertical motion has higher frequency than the horizontal ground motion. It should be noted that the fundamental period of the structure in the horizontal direction is usually much higher than the vertical direction.

A comparison for horizontal and vertical component of Northridge earthquake (1994) at the Sylmar converter station is presented in Fig. 2. The figure shows the response spectra and the frequency response, which represents the energy content of ground motion. This figure confirms that higher frequency content is usually observed in vertical ground motion components, compared with horizontal motion. Although the energy content over the frequency range of the vertical ground motion is lower than that of the horizontal ground motion, it has a tendency to concentrate all its energy in a narrow, high frequency band as depicted in Fig. 2. Therefore, such high frequency content leads to large amplifications in the short period range, which often coincide with the vertical mode of RC structure, thus causing significant response amplification.

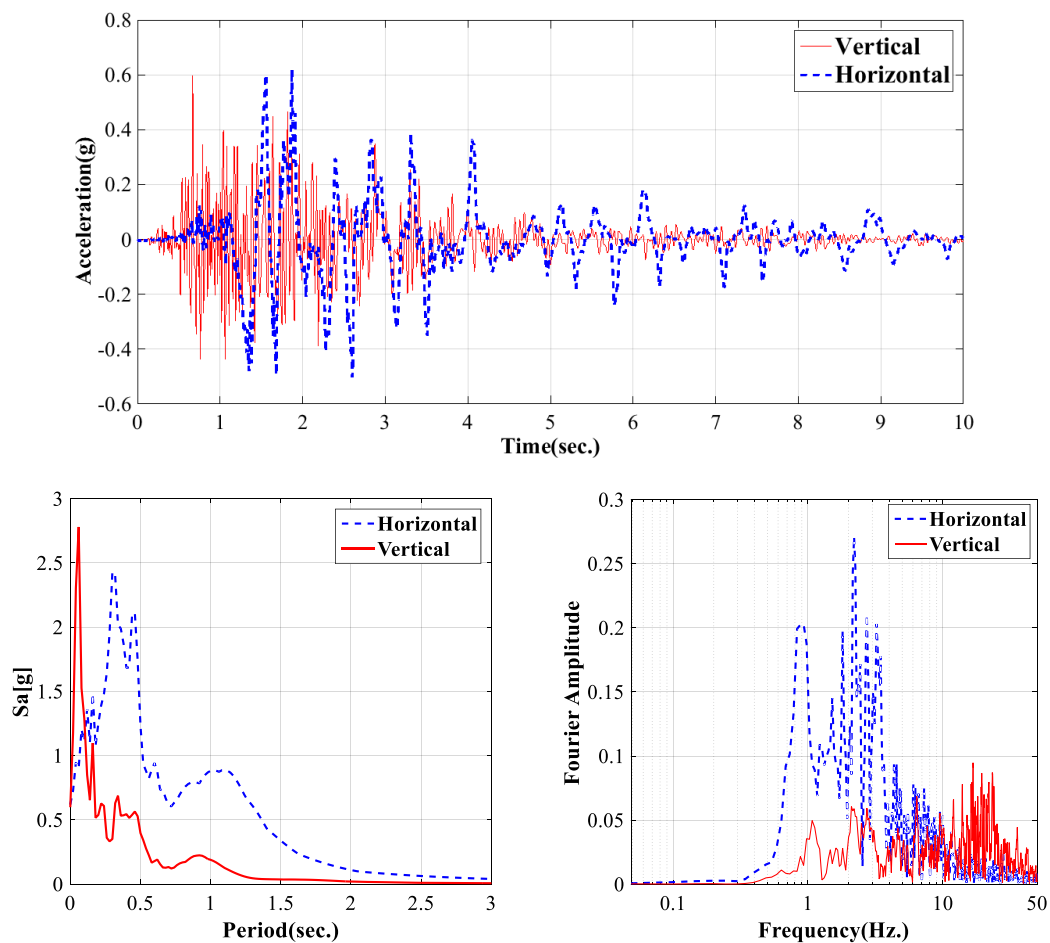


Fig. 2 Comparison of horizontal and vertical ground excitations frequency content for Northridge earthquake

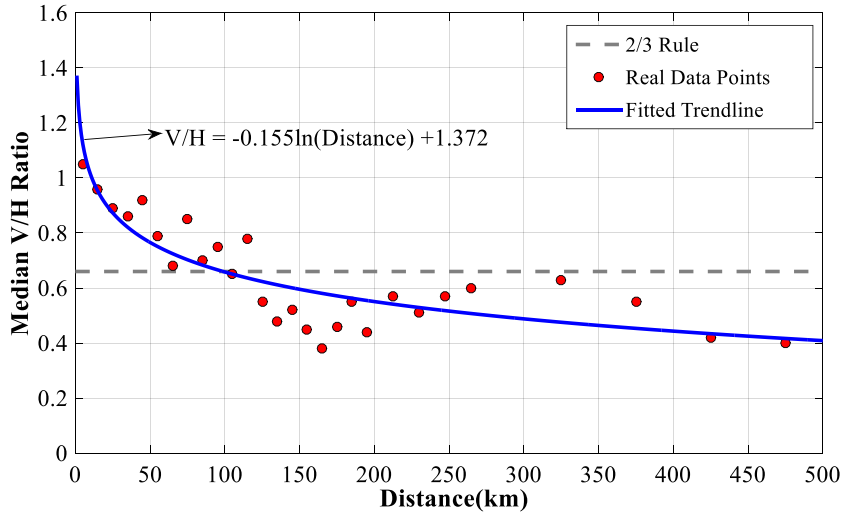


Fig. 3 Median V/H ratio vs. the epi-central distance

Currently, most of the building codes consider the vertical to horizontal (V/H) ratio of the acceleration spectra to be 2/3. However, Bozorgnia and Campbell (2004) has showed that the acceleration spectra at short period are generally larger than 2/3. On the other hand, V/H ratio is generally lower in the higher structural period. Hence, the use of the 2/3 value might not be appropriate for all cases. To further study the influence of the vertical ground motion compared to the horizontal ground motion, the ratio of the peak vertical ground acceleration vs. the peak horizontal ground acceleration as a function of the Epi-central distance is presented in Fig. 3. To filter the ground motions with insignificant impact on the structural response, the ground motion with small spectral acceleration ($Sa(T_1, H) < 0.1$ g) for all period less than 4 second are removed. This reduces the available ground motion from 21,000 to 1,700 records. The result shows as the distance increases, the influence of the vertical to horizontal peak ground motion decreases. For distance less than 100 km, the assumption that the peak vertical ground motion is 2/3 of the horizontal ground motion is unrealistic and should be modified.

4. Ground motions selection

Based on the information presented in the previous section, ground motions were selected from the PEER NGA-WEST2 database (Ancheta *et al.* 2013) and Iran Strong Motions Network (<http://smd.bhrc.ac.ir/Portal/en/Search/Waveforms>). These databases contain more than 20,000 earthquake records. To limit the scope of the analysis, only ground motion with specific criteria, as shown in Table 3, are selected. The first selection criterion eliminates the earthquakes with small shaking intensities. Ground motions with horizontal spectral acceleration ($Sa(T_1)$) in either directions less than 0.10 g were eliminated. This quickly reduced the eligible ground motions to 1,778 records. The second selection criterion eliminate the records that are far field motions. As the result presented in Fig. 3, the vertical component of the ground motion is most significant in the near-field range, hence ground motion recorded with Epi-central distance (EpiD) greater than

Table 3 Ground motion selection criteria

Case	Criteria
1	$Sa_{\max,H} \geq 0.1 \text{ g}$
2	Distance to the fault $\leq 25 \text{ km}$
3	$M_w \geq 6.0$
4	$Sa_{H \text{ or } V} \geq 0.01 \text{ g}, (T = 0-4 \text{ sec})$

Table 4 Summary of the ground motions selected (Sorted by Magnitude)

No.	Earthquake Name	Date	Station Name	Moment Magnitude, M_w	EpiCentral Distance, (km)	(PGA) _H , g	(PGA) _V , g
1	Wenchuan, China	2008	Wenchuanwolong	7.90	19.54	0.77	0.96
2	Chi-Chi, Taiwan	1999	TCU078	7.62	4.96	0.38	0.17
3	Chi-Chi, Taiwan	1999	TCU089	7.62	14.16	0.75	0.34
4	Chi-Chi, Taiwan	1999	TCU079	7.62	15.42	0.59	0.42
5	Kocaeli, Turkey	1999	Izmit	7.51	5.31	0.19	0.14
6	Kocaeli, Turkey	1999	Yarimca	7.51	19.30	0.29	0.24
7	Tabas, Iran	1978	Dayhook	7.35	20.63	0.33	0.19
8	Landers, US	1992	Joshua Tree	7.28	13.67	0.27	0.18
9	Landers, US	1992	Morongo Valley Fire Station	7.28	21.34	0.19	0.16
10	Duzce, Turkey	1999	Duzce	7.14	1.61	0.43	0.35
11	Duzce, Turkey	1999	Lamont 1058	7.14	24.05	0.68	0.19
12	Duzce, Turkey	1999	IRIGM 487	7.14	24.31	1.00	0.33
13	Golbaft, Iran	1981	Golbaft	7.00	13.00	0.28	0.24
14	Darfield, New Zealand	2010	GDLC	7.00	4.42	0.73	1.25
15	Darfield, New Zealand	2010	HORC	7.00	10.91	0.47	0.81
16	Loma Prieta, US	1989	Corralitos	6.93	7.17	0.50	0.46
17	Loma Prieta, US	1989	BRAN	6.93	18.46	0.59	0.90
18	Loma Prieta, US	1989	Capitola	6.93	20.35	0.44	0.14
19	Kobe, Japan	1995	Nishi-Akashi	6.90	8.70	0.47	0.39
20	Kobe, Japan	1995	IWTH26	6.90	13.12	0.67	0.28
21	Kobe, Japan	1995	Takatori	6.90	19.25	0.32	0.57
22	Nahanni, Canada	1985	Site 2	6.76	6.52	0.40	0.67
23	Nahanni, Canada	1985	Site 1	6.76	6.80	1.16	2.28
24	Northridge, US	1994	Rinaldi Receiving	6.69	5.41	1.64	1.05
25	Northridge, US	1994	Arleta - Nordhoff Fire Sta	6.69	8.48	0.75	0.32
26	Northridge, US	1994	LA Dam	6.69	20.36	1.39	1.23
27	Niigata, Japan	2004	NIG019	6.63	4.36	1.26	0.80
28	Niigata, Japan	2004	NIG020	6.63	21.52	1.48	0.57
29	Bam, Iran	2003	Bam	6.60	12.59	0.74	0.97
30	Zarand, Iran	2005	Zarand	6.40	16.00	0.31	0.30

Table 4 Continued

31	Imp. Valley, US	1979	Bonds Corner	6.53	6.19	0.69	0.53
32	Imp. Valley, US	1979	Calexico Fire Station	6.53	19.44	0.31	0.25
33	Imp. Valley, US	1979	Chihuahua	6.53	24.82	0.17	0.21
34	Christchurch, New Zealand	2011	Heathcote Valley Primary School	6.20	1.11	1.39	2.18
35	Christchurch, New Zealand	2011	LPCC	6.20	4.89	0.65	1.90
36	Morgan Hill, US	1984	Halls Valley	6.19	16.67	0.35	0.21
37	Morgan Hill, US	1984	Zack Brothers Ranch	6.19	24.55	0.94	0.39
38	Talesh, Iran	1978	Talesh	6.00	15.00	0.23	0.13
39	Parkfield, US	2004	Parkfield - Stone Corral 1E	6.00	7.17	0.72	0.33
40	Parkfield, US	2004	Parkfield - Stone Corral 2E	6.00	9.28	0.83	0.72

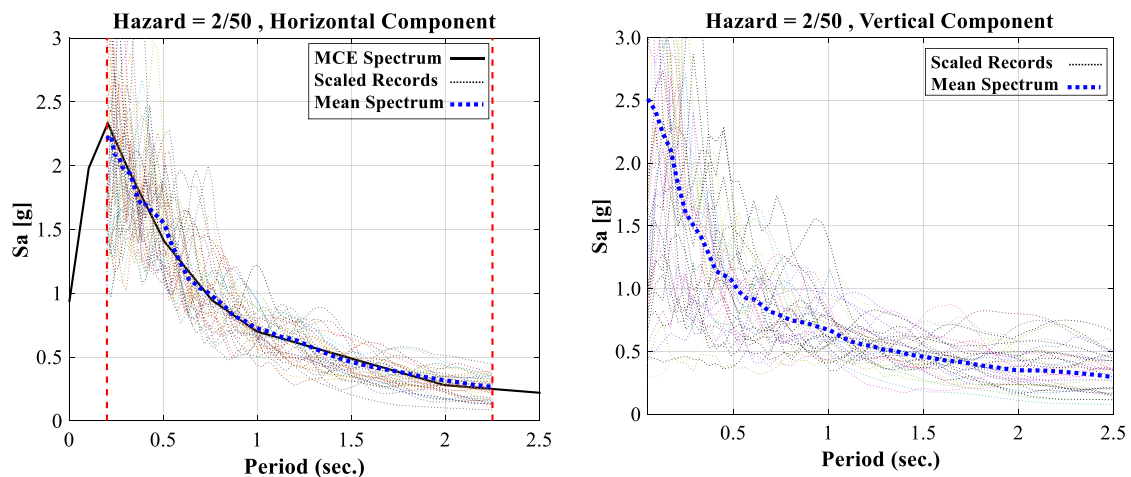


Fig. 4 Scaled horizontal and vertical spectrum with the same scaling factor.

25 km were eliminated. This further reduced the eligible ground motions to 737 records. The third criterion is used to eliminate the ground motion with moment magnitude (M_w) less than 6.0, which removes the effect of non-destructive events. The last criterion filters the ground motion with very small spectral acceleration values. The final dataset consists of 298 records, of which 40 ground motion records from 20 earthquake events have been extracted and used in this study. Table 4 shows the summary of the ground motion selected for this study.

After the ground motions were selected, the records were amplitude scaled to match the 5% damped site-specific target spectrum (corresponds to the maximum credible earthquake hazard level) retrieved from the United States Geological Survey (<http://geohazards.usgs.gov/hazardtool/>). The ground motions were amplitude scaled within the period range from $0.2 T_{1\text{short}}$ to $1.5 T_{1\text{long}}$, where $T_{1\text{short}}$ and $T_{1\text{long}}$ are the shortest and longest fundamental periods of the buildings,

respectively. As shown in Table 2, the shortest building period is 0.98 sec and the longest building period is 1.49 sec. This scaling procedure is similar to the ground motion scaling procedure as outlined in ASCE 7 (ASCE 2010). Fig. 4(a) shows the scaled response spectrum for the horizontal ground motions used for this study. Fig. 4(b) shows the spectral acceleration of the vertical component with the same scaling factor. The result shows the mean vertical spectrum is higher than the mean horizontal spectrum.

As the structure has different vertical and horizontal vibrational period (see Table 2), the vertical spectra acceleration at the vertical mode of vibration is compared to the horizontal spectra acceleration at the horizontal mode of vibration and presented in Fig. 5. The solid red lines indicate the median ratio (50% probability), while lower and upper boundary lines show the 10% and 90% probability of the data. The remaining data points plotted by red markers are the outliers. The result shows the vertical spectra acceleration at the vertical vibration mode are higher than the horizontal spectra acceleration at the horizontal vibration mode. This effect is even more significant for the taller buildings.

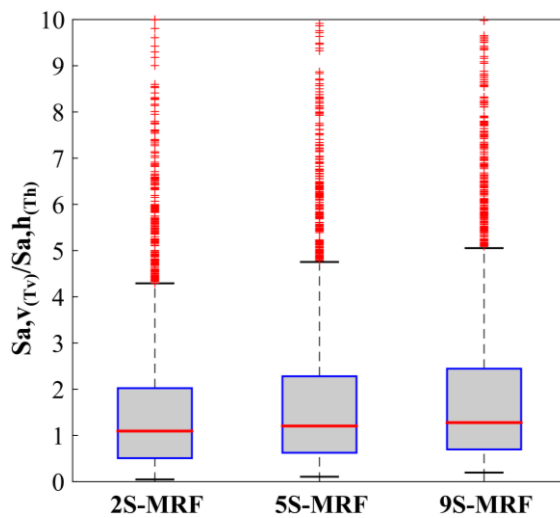


Fig. 5 V/H spectra acceleration ratios at the fundamental period of the structures based on NGA-WEST2 dataset

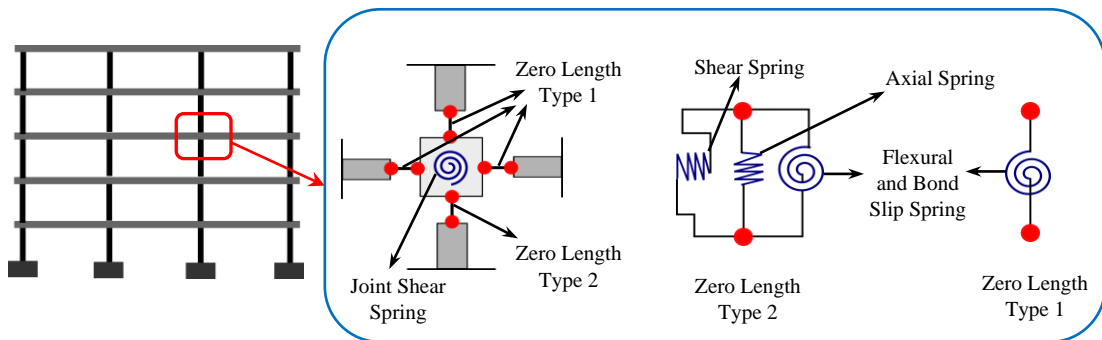


Fig. 6 Schematic representation of the finite element models developed in OpenSees

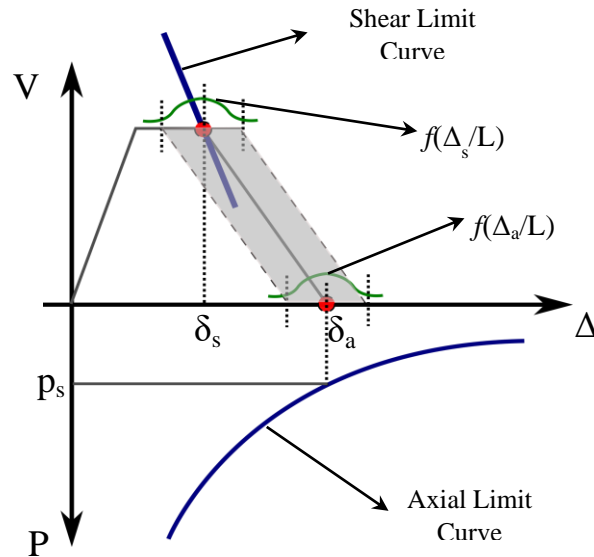


Fig. 7 Limit State material model and corresponding uncertainties in axial and shear failure models (Elwood 2004)

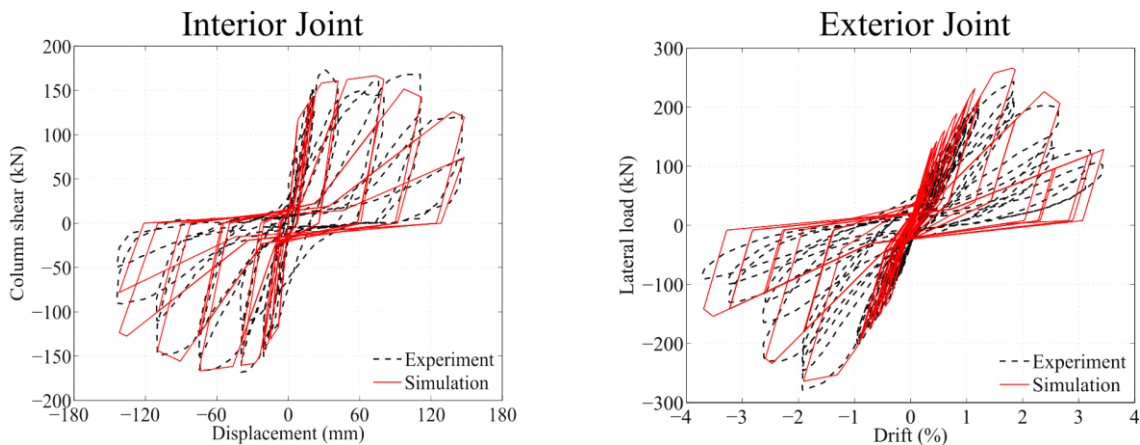


Fig. 8 Joints calibrated through experimental results (Hakuto *et al.* 2000, Clyde *et al.* 2000)

5. Modeling of the prototype buildings

Nonlinear dynamic models for each of the prototype buildings were developed using OpenSees (McKenna 2014). Fig. 6 shows the schematic view of the finite element models developed.

The non-ductile behavior of the RC columns was developed using zero-length elements, where axial and shear response were coupled using the Limit State material in OpenSees which was developed by (Elwood 2004). Each Limit State material model uses a drift capacity model to determine the point of shear or axial failure. As shown in Fig. 7 the shear limit curve is activated and shear failure is initiated as the column deformation exceed the deformation capacity. To account for uncertainties, a lognormal distribution was used to quantify the model parameters. The

shaded area shown in Fig. 7 presents the range of the model variability considered for these non-ductile columns.

The beams and columns were modeled as elastic element, where the nonlinearity in flexural responses were lumped in the joints. The joints were modeled using nonlinear shear hinge where the failure can be modeled using degrading model developed by Ibarra *et al.* (2005). The calibration of the numerical models was calibrated against the RC columns experimental data by Haselton *et al.* (2008). Fig. 8 shows the calibrated joints data. Masses were lumped at the beam-column joints in both horizontal and vertical directions. Geometry nonlinearity were modeled using the $P-\Delta$ transformation. 2% Rayleigh tangent stiffness and mass proportional was assigned in the first 2 horizontal modes of vibration.

6. Results and discussion

6.1 Effect of vertical excitations on the structural responses (member level)

The vertical ground motions can increase the fluctuation of the axial forces in columns. Since the flexural and shear behavior of reinforced concrete columns are coupled with the axial force, the fluctuation in axial forces may cause significant variation in stiffness and strength of the columns. In some extreme cases, this may result in extensive damages to the structural columns. Figs. 9 to 11 shows the axial forces in the 1st storey interior column for the 5 storey model, when subjected to Northridge GM under varying vertical ground excitations. To emphasize the influence of the vertical shaking on the response of the column, the shear capacity of the column was calculated using the formula as presented in Priestley *et al.* (1996). This model account for the shear strength degradation as a function of column displacement or curvature ductility. The result shows when the $V/H_{Record}=0.00$, the structure does not experience shear failure (Fig. 9). However,

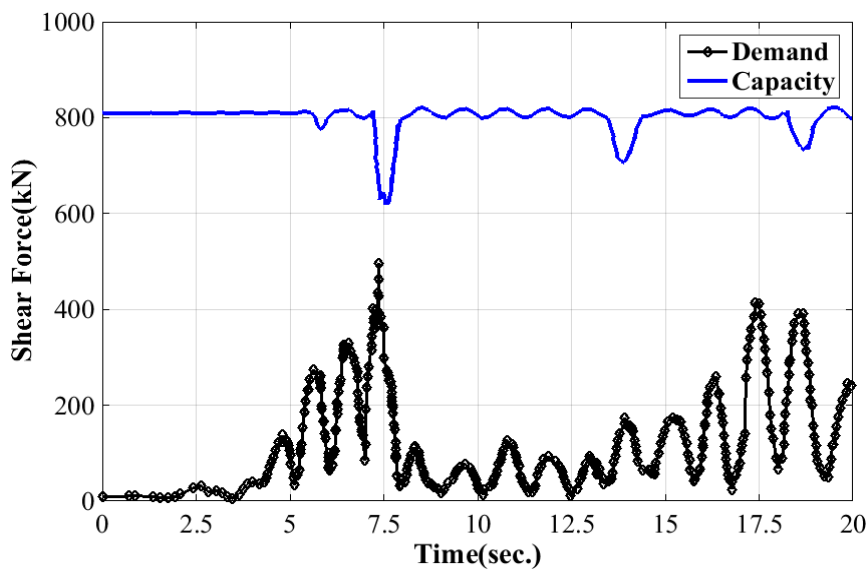


Fig. 9 Shear capacity and demand of 2nd column at 1st storey of 5S-MRF [$(V/H)_{Record} \approx 0.00$]

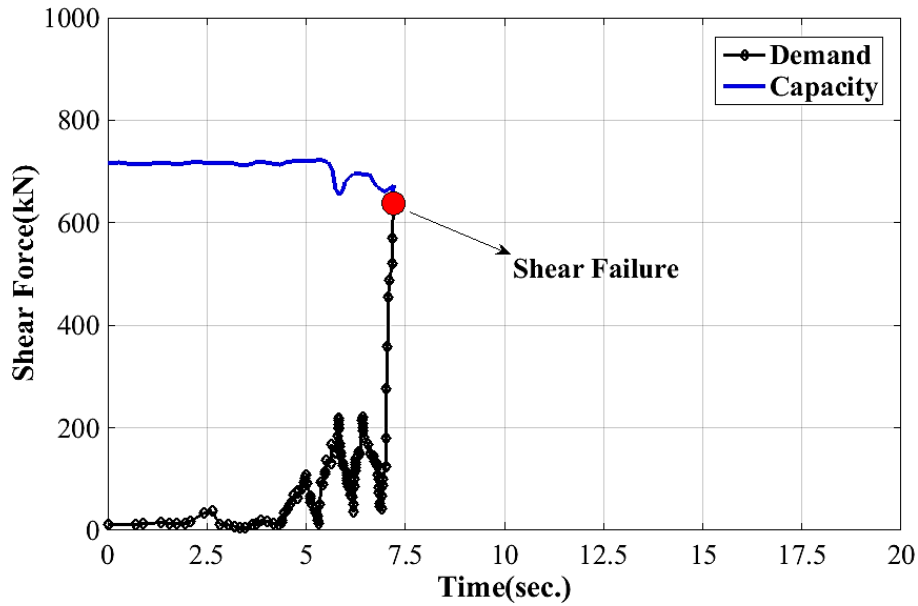


Fig. 10 Shear capacity and demand of 2nd column at 1st storey of 5S-MRF [(V/H)_{Record} ≈ 4/3 = 1.33]

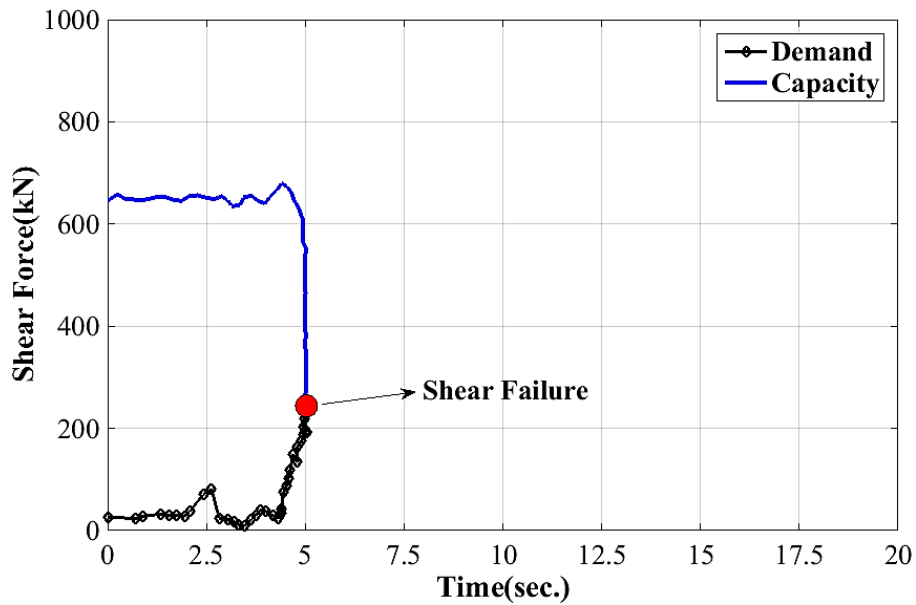


Fig. 11 Shear capacity and demand of 2nd column at 1st storey of 5S-MRF [(V/H)_{Record} ≈ 6/3 = 2.00]

when the $V/H_{Record}=4/3$, the shear demand increases at the same time the shear capacity dropped. The shear failure happened when $t=7$ sec (Fig. 10). When the $V/H_{Record}=2.00$, the shear failure happened sooner when $t=5$ sec (Fig. 11). The results show that the shear demand exceeds the capacity when vertical ground motion is included. Similar behavior is observed in the 2 and 9 storey models. Therefore, it could be concluded that the columns are more susceptible to shear

Table 5 Average shear capacity and demand for various V/H of the inner columns at 1st storey

Model	V/H	Shear Capacity (kN)	Shear Demand (kN)	Reduction in Capacity (%)	Increase in Demand (%)
2S-MRF	0.00 (H Only)	381	98	(Reference)	(Reference)
	4/3=1.33	312	108	-18.11%	10.20%
	6/3=2.00	267	115	-29.92%	17.35%
5S-MRF	0.00 (H Only)	775	147	(Reference)	(Reference)
	4/3=1.33	615	168	-20.65%	14.29%
	6/3=2.00	478	179	-38.32%	21.77%
9S-MRF	0.00 (H Only)	1351	280	(Reference)	(Reference)
	4/3=1.33	1027	325	-23.98%	16.07%
	6/3=2.00	712	348	-47.30%	24.29%

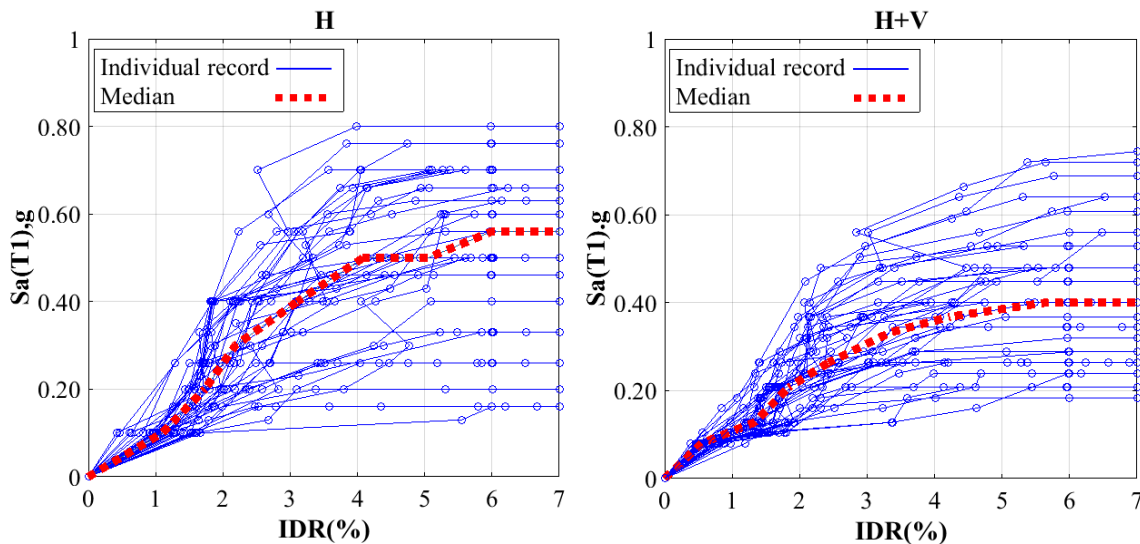


Fig. 12 IDA curves under horizontal and H+V excitations (5S-MRF)

failure, when the vertical component of ground motion is included. For a better comparison, the fluctuations in shear demand and capacity of all the studied structures are given in Table 5.

6.2 Incremental dynamic analysis

In addition to nonlinear time history analysis presented in the previous section, incremental dynamic analyses (IDA) were used to examine the collapse margin ratio (CMR) of the prototype buildings. Two collapse modes, side sway and gravity collapse were considered. Side-sway failure was defined when the IDA curve may become a flat line, which means that the solution has not converged completely and the structure becomes unstable. This is consistent with the approach suggested by Cornell *et al.* (2005). Fig. 12(a) and Fig. 12(b) show the comparison of the IDA curve for the 5-story model without and with the vertical ground motion, respectively. As

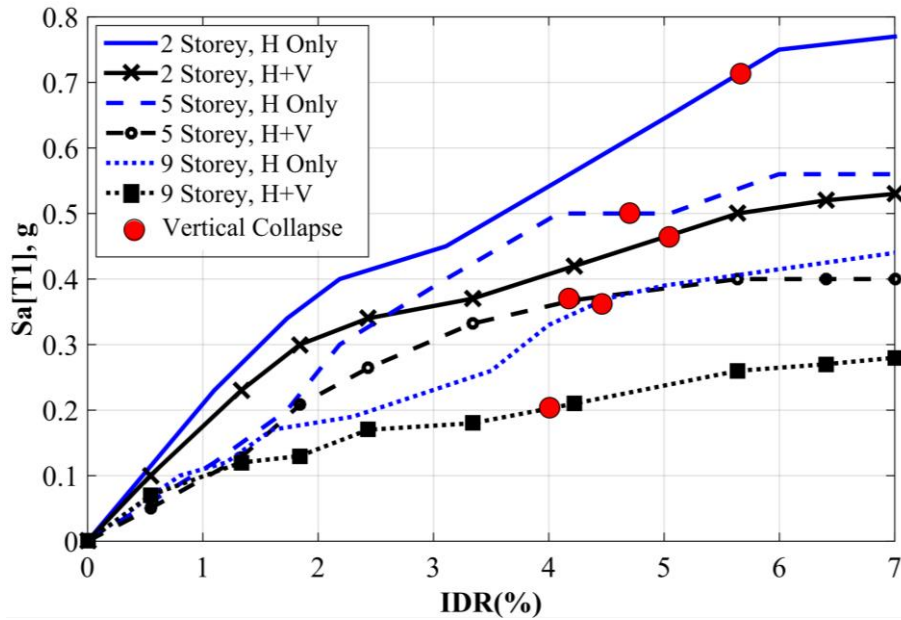


Fig. 13 Combined side-sway and gravity collapse results

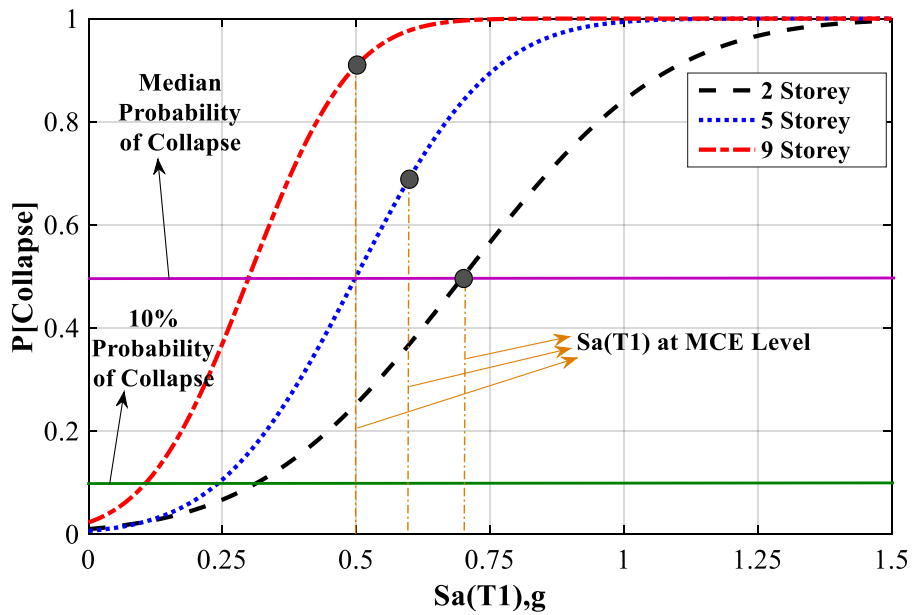


Fig. 14 Collapse indicators on the fragility curves under horizontal excitation

illustrated from these figures, the median IDA curves changed significantly when the vertical component of the ground motion are included. Fig. 13 shows the summary of the IDA curves for the 3 different building heights. The result shows collapse happens sooner when the vertical ground motion is included. Similarly, collapse happen sooner on the tall building.

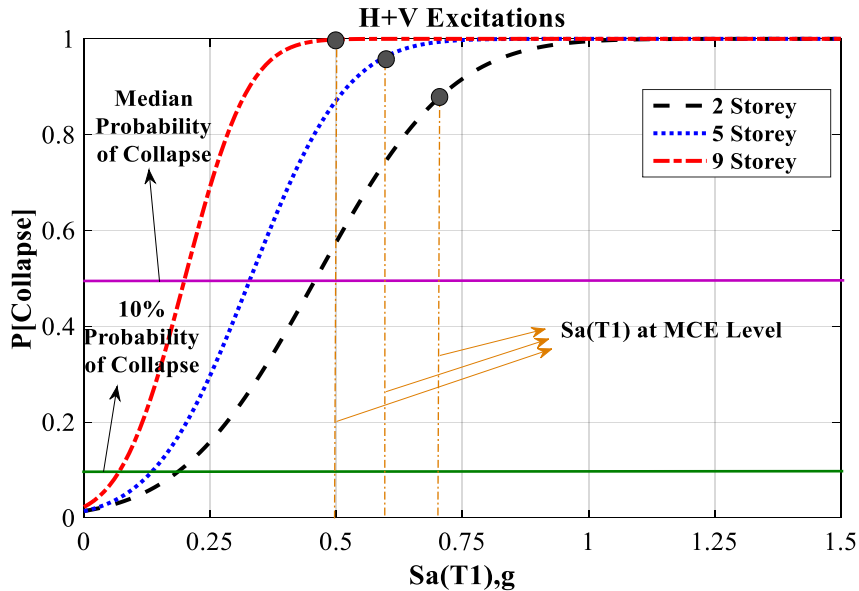


Fig. 15 Collapse indicators on the fragility curves under combined H+V excitation

Table 6 Collapse performance metrics for the studied RC-MRFs

Model	T_1 (sec.)	$Sa(T_1)$ @ MCE (g)	Eq. Type	$P[\text{Collapse}]$ @ $Sa(T_1)$	$Sa(T_1)$ @ Median Probability of Collapse	CMR
2 Storey			H	50%	0.70	0.99
			H+V	88%	0.43	0.61
5 Storey			H	69%	0.49	0.79
			H+V	94%	0.33	0.53
9 Storey			H	91%	0.29	0.60
			H+V	100%	0.20	0.41

6.3 Collapse margin ratio (CMR)

Fig. 14 and Fig. 15 show the probability of collapse without and with vertical ground motion at different shaking intensities, respectively. The result shows the probability of collapse increases significantly when the vertical ground motions are included. The collapse margin ratios (CMR) for the 2, 5 and 9 story non-ductile RC-MRFs for the different seismic excitations are and presented in Table 6. The result shows that the collapse probability at $Sa(T_1)$ is much higher for the case of combined horizontal-vertical excitation compared to the case of horizontal only excitations. These differences are in the range of 9% to 38% for the considered archetypical buildings. On the other hand, the calculated collapse margin ratios (CMRs) are significantly less for the case where both the H+V excitations are included, which confirm the fact that multi-components excitations will be highly important for the case of non-ductile RC-MRFs. The result also shows as the story height increases, the collapse probability increases. Hence, the 9-storey RC building has higher collapse probability than the 2-storey RC building.

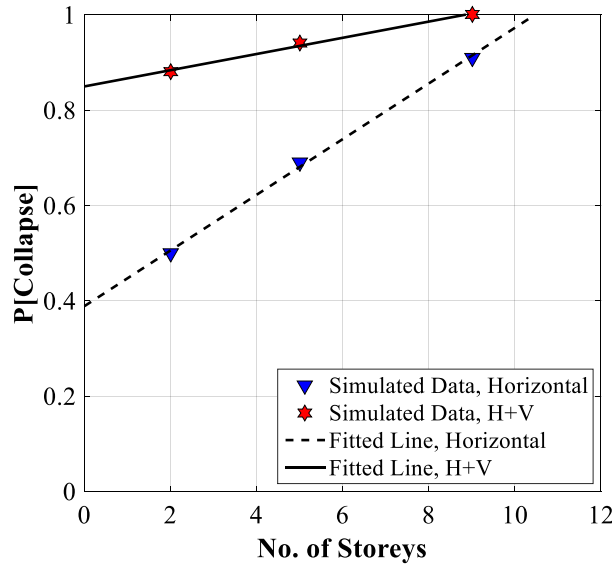


Fig. 16 Probability of collapse vs. the spectral acceleration at MCE level

Fig. 16 shows the summary of the probability of collapse as a function of the storey number. Coincidentally, the probability of collapse increases as the number of structure increases.

Based on the data presented in Fig. 16, two equations are derived to show the correlation between probability of collapse in non-ductile RC frames, the number of storeys, and the spectral acceleration at the first mode period of considered structures at MCE level (Eqs. (1) and (2)). These formulas can be used for a rough estimate of other non-ductile RC frames having only the number of storeys. It would be very useful for the practical engineers and designers to include the effect of vertical excitation to confirm the safety of their structure.

$$P[\text{Collapse}]_{\text{Horizontal,Excitation}} = 0.0584 \times (\text{No.of .Storeys}) + 0.389 \quad (1)$$

$$P[\text{Collapse}]_{(\text{H+V}),\text{Excitation}} = 0.017 \times (\text{No.of .Storeys}) + 0.85 \quad (2)$$

7. Conclusions

In this study, the influence of the vertical ground motion on the collapse fragility of non-ductile RC frames was performed. Prototype building with varying heights (2-, 5- and 9-stories) were designed according to the 1967 Uniform Building Code. Robust finite element models were developed in OpenSees. A suite of 40 ground motions was selected from the PEER and BHRC database. Detailed nonlinear IDA were performed. The results show:

- Near-field records have higher vertical excitations than the far-field records. In general, the V/H ratio are higher than 2/3 when the epi-central distance is less than 100km.
- Vertical ground excitations have lower energy content than their horizontal counterparts, these energies are concentrated in a narrow band in the high frequency range. This may cause

significant damages to (mid and high)-rise RC-MRFs.

- Extracted collapse margin ratio (CMR) and collapse fragility curves showed that non-ductile RC-MRFs are very vulnerable to vertical ground shaking and the seismic assessment need to include such an effect.
- Significant increase of axial force variation due to vertical ground motion leads to an observed reduction of shear capacity in the range of 18-48%. This increases the shear demand in the range of 10-24%. This increase the probability of shear failure in columns and hence the collapse mechanism of the structure.
- The probability of collapse increases as a function of story height and the impact of vertical ground motion excitation is much more significant in the high rise building.
- A simple formula is proposed based on the result presented in this study, this formula allows the engineers to quantify the collapse vulnerability of non-ductile RC building with and without considering the vertical excitation.

These finding confirmed that the non-ductile RC buildings located near the active faults are vulnerable to combined vertical and horizontal shaking, hence, it is crucial to include the combined vertical and horizontal shaking during the seismic design and assessment of non-ductile RC moment frames.

References

- Anagnos, T., Comerio, M.C., Goulet, C., Na, H., Steele, J. and Stewart, J.P. (2008), "Los Angeles inventory of non-ductile concrete buildings for analysis of seismic collapse risk hazards", *Proc. 14th World Conf. Earthquake Eng.*, 12-17.
- Ancheta, T.D., Darragh, R.B., Stewart, J.P., Seyhan, E., Silva, W.J., Chiou, B.S.J., ... & Donahue, J.L. (2013), "PEER NGA-West2 Database", PEER Report, **3**, 83.
- ASCE (2010), "Minimum design loads for buildings and other structures, ASCE Standard ASCE/SEI 7-10", American Society of Civil Engineers: Reston, Virginia.
- Bommer, J., Bray, J.D., Pitilakis, K. and Yasuda, S. (2005), *Geotechnical, geological and earthquake engineering*, Springer.
- Bozorgnia, Y. and Campbell, K.W. (2004), "The vertical-to-horizontal response spectral ratio and tentative procedures for developing simplified V/H and vertical design spectra", *J. Earthq. Eng.*, **8**, 175-207.
- Clyde, C., Pantelides, C.P. and Reaveley, L.D. (2000), "Performance-based evaluation of exterior reinforced concrete building joints for seismic excitation", PEER Report 2000/05, Pacific Earthquake Engineering Center, University of California, Berkeley, CA.
- Code, UBC (1967), Edition, Vol. I, In International Conference of Building Officials, Pasadena, California.
- Collier, C.J. and Elnashai, A.S. (2001), "A procedure for combining vertical and horizontal seismic action effects", *J. Earthq. Eng.*, **5**(4), 521-539.
- Cornell, A., Zareian, F., Krawinkler, H. and Miranda, E. (2005), "Prediction of probability of collapse, van Nuys hotel building testbed report: exercising seismic performance assessment", *Pacific Earthq. Eng. Res.*, **11**, 85-93.
- Elwood, K.J. (2004), "Modelling failures in existing reinforced concrete columns", *Can. J. Civil Eng.*, **31**(5), 846-859.
- Eskandari, R. and Vafaei, D. (2015), "Effects of near-fault records characteristics on seismic performance of eccentrically braced frame", *Struct. Eng. Mech.*, **56**(5), 855-870.
- Galal, K. (2007), "Lateral force-displacement ductility relationship of non-ductile squat RC columns rehabilitated using FRP confinement", *Struct. Eng. Mech.*, **25**(1), 75-89.
- Hakuto, S., Park, R. and Tanaka, H. (2000), "Seismic load tests on interior and exterior beam-column joints

- with substandard reinforcing details”, *ACI Struct. J.*, **97**(1), 11-25.
- Haselton, C., Liel, A., Taylor Lange, S. and Deierlein, G.G. (2008), “Beam-Column element model calibrated for predicting flexural response leading to global collapse of RC frame buildings”, PEER Rep. 2007/03, Pacific Earthquake Engineering Research Center (PEER), Univ. of California at Berkeley, Berkeley, CA.
- Ibarra, L.F., Medina, R.A. and Krawinkler, H. (2005), “Hysteretic models that incorporate strength and stiffness deterioration”, *Earthq. Eng. Struct. Dyn.*, **34**(11), 1489-1511.
- Iranian Building and Housing Research Center website, www.bhrc.ac.ir
- Liel, A.B. and Deierlein, G.G. (2008), “Assessing the collapse risk of California’s existing reinforced concrete frame structures: metrics for seismic safety decisions”, Blume Earthquake Engineering Center, No. 166, Stanford University.
- Liel, A.B., Haselton, C.B. and Deierlein, G.G. (2011), “Seismic collapse safety of reinforced concrete buildings: ii. comparative assessment of non-ductile and ductile moment frames”, *J. Struct. Eng.*, **137**(4), 492-502.
- McKenna, F. (2014), “Open system for earthquake engineering simulation (OpenSees)”, Version 2.4. 4 MP.
- Papazoglou, A.J. and Elnashai, A.S. (1996), “Analytical and field evidence of the damaging effect of vertical earthquake ground motion”, *Earthq. Eng. Struct. Dyn.*, **25**, 1109-1137.
- Prager, F., Tucker, J. and Sneider, L.P. (2009), “The policy problem of non-ductile concrete buildings in Los Angeles: Costly earthquakes, uncertain owners”, *ASCE/SEI Conference on Improving the Seismic Performance of Existing Buildings and Others Structures*.
- Priestley, M.J.N., Benzoti, G., Ohtaki, T. and Seible, F. (1996), “Seismic performance of circular reinforced concrete columns under varying axial load”, Report-SSRP-96/04, Division of Structural Engineering, University of California, San Diego, CA.
- United States Geological Survey website, www.usgs.gov
- Wen, Y.K., Ellingwood, B.R. and Bracci, J.M. (2004), “Vulnerability functions”, Technical Rep., DS-4, Mid-America Earthquake Center, Univ. of Illinois at Urbana- Champaign.
- Zhang, B., Yang, Y., Wei, Y.F., Liu, R.Y., Ding, C. and Zhang, K.Q. (2015), “Experimental study on seismic behavior of reinforced concrete column retrofitted with prestressed steel strips”, *Struct. Eng. Mech.*, **55**(6), 1139-1155.